Available online at www.sciencedirect.com

ScienceDirect

journal homepage: www.elsevier.com/locate/he

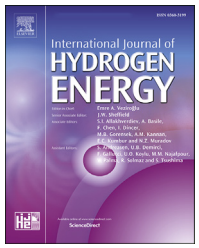

# The instability of laminar methane/hydrogen/air flames: Correlation between small and large-scale explosions

*Mohamed E. Morsy* [a,b], *Junfeng Yang* [a,*]

[a] *School of Mechanical Engineering, University of Leeds, Leeds LS2 9JT, United Kingdom*
[b] *Faculty of Engineering at El-Mattaria, University of Helwan, Cairo 11718, Egypt*

## HIGHLIGHTS

- Onset of instabilities of methane/hydrogen/air flames was studied and presented.
- Flame speeds, critical radius, Karlovitz factor and strain rates were derived.
- Correlations between small and large scale were developed and presented.
- Such correlations can predict the instability in large-scale atmospheric explosions.
- Effects of pressure and hydrogen fraction on the onset of instability were analyzed.

## ARTICLE INFO

*Article history:*
Received 10 May 2022
Received in revised form
15 June 2022
Accepted 28 June 2022
Available online 13 August 2022

*Keywords:*
Flame instability
Laminar burning velocity
Hydrogen
Methane
Large-scale explosions

## ABSTRACT

Darrieus–Landau (D-L) instability can cause significant acceleration in freely expanding spherical flames, which can lead to accidental large-scale gas explosions. To evaluate the potential of using high-pressure lab-scale experiments to predict the onset of cellular instabilities in large-scale atmospheric explosions, experimental measurements of the cellular instabilities for hydrogen and methane mixtures are conducted, in laboratory spherical explosions at elevated pressures. These measurements are compared with those from several large-scale atmospheric experiments. Comprehensive correlations of the pressure effect on a critical Karlovitz number, $K_{cl}$, together with those of strain rate Markstein number, $Ma_{sr}$, are developed for hydrogen/air mixtures. The regime of stability reduces for all mixtures, as $Ma_{sr}$ becomes negative. Values derived from large-scale experiments closely follow the same correlation of $K_{cl}$ with $Ma_{sr}$. As a result, the extent of the regime where the laminar explosion flames become unstable can be predicted as a function of $Ma_{sr}$ and pressure.

© 2022 The Author(s). Published by Elsevier Ltd on behalf of Hydrogen Energy Publications LLC. This is an open access article under the CC BY license (http://creativecommons.org/licenses/by/4.0/).

* *Corresponding author.*
E-mail address: J.Yang@leeds.ac.uk (J. Yang).

https://doi.org/10.1016/j.ijhydene.2022.06.289

0360-3199/© 2022 The Author(s). Published by Elsevier Ltd on behalf of Hydrogen Energy Publications LLC. This is an open access article under the CC BY license (http://creativecommons.org/licenses/by/4.0/).

**Nomenclature**

| | |
|---|---|
| $C_P$ | specific heat at constant pressure (J/kg/K) |
| $K_{cl}$ | critical Karlovitz number, Eq. (4) |
| $K$ | turbulent Karlovitz stretch factor |
| $L_b$ | burned gas Markstein length (m) |
| $Le$ | Lewis number, Eq. (9) |
| $Ma_b$ | flame speed Markstein number |
| $Ma_{sr}$ | strain rate Markstein number |
| $n$ | Theoretical wave number |
| $P$ | Pressure |
| $P_a$ | atmospheric pressure (Pa) |
| $Pe_{cl}$ | critical Peclet number |
| $Pr$ | $(C_p\eta/k)$, Prandtl number |
| $r_u$ | flame radius (m) |
| $r_{cl}$ | critical flame radius (m) |
| $S_n$ | stretched flame speed (m/s) |
| $S_s$ | unstretched flame speed (m/s) |
| $t$ | time (s) |
| $u_l$ | unstretched laminar burning velocity (m/s) |
| $u_n$ | stretched laminar burning velocity (m/s) |

*Greek symbols*

| | |
|---|---|
| $\alpha$ | flame stretch rate (1/s) |
| $\delta_l$ | laminar flame thickness (m) |
| $\nu$ | viscosity (N.s/m$^2$) |
| $k$ | thermal conductivity (W/m/K) |
| $n$ | kinematic viscosity (m$^2$/s) |
| $\Lambda$ | Normalized wavelength |
| $\rho_b$ | density of burned gas (kg/m$^3$) |
| $\rho_u$ | unburned gas density (kg/m$^3$) |
| $\sigma$ | thermal expansion ratio |
| $\varphi$ | equivalence ratio |

*Subscripts*

| | |
|---|---|
| $b$ | burned |
| $cl$ | critical |
| $sr$ | strain rate |
| $u$ | unburned |

## Introduction

The cellular instability of methane/hydrogen ($CH_4/H_2$) blends have been extensively studied, mostly focused on the flame self-acceleration [1–3], cellular structure [4–8] and onset of instabilities [3,6,8–11]. It was found that, as $H_2$ fraction increases in the mixture, the instabilities become significant and increase the flame speed as a result of the high preferential diffusion of hydrogen [12], especially at high initial pressures [8]. This also has been attributed to both Lewis number and flame thickness. The flame thickness of $H_2$/air flames is relatively small, smaller than that of $CH_4$/air flames, and Lewis number of $H_2$/air flames is less than unity, in the lean side, which lead the $CH_4/H_2$/air flame to be more unstable with increasing hydrogen fraction. Hu et al. [13] studied the effect of initial pressure and initial temperature on the instability of $CH_4/H_2$/air flames. Hu found that the critical radius increases with initial pressure as a result of the enhancement in hydrodynamic instability, while Markstein length decreases significantly with increasing $H_2$ fraction in the mixture. The effect of the initial temperature on the flame instability was negligible. Recently, more attention has been paid to the explosion pressure rise rate of $CH_4/H_2$/air mixtures [14–17]. Salzano et al. [18] showed that the pressure increases significantly with increasing $H_2$ fraction in the mixture, regardless of the initial pressure. This is in a good agreement with [19]. Chen et al. [19] attributed the increase in the explosion pressure to the flame instability, which could significant increase the flame propagation speed and hence the pressure. Furthermore, it has been reported that the turbulent burning velocity can be enhanced by flame instability [20–26]. The majority of the above mentioned work involves laminar explosion flames in laboratory-closed vessels (bombs) and the cellular instabilities of $H_2$ flames have been widely reported. These instabilities can be serious in large-scale (LS) explosions, initiated in quiescent premixed gases. In the 1970s, a number of studies of LS explosions was initiated due to concerns about the potential consequences of LS explosions associated with bulk transportation of liquefied natural gas (LNG) [22,27]. More recently, several measurements were conducted by Shell Research Ltd. as a part of the SOLVEX program [28] to study LS explosions, related to the safety of offshore units for the oil and gas industries. Yet it is still not clear whether the instabilities of hydrogen/methane/air flames that appear in small, high pressure, laboratory measurements in closed combustion vessels, can be used to predicate those appear in LS atmospheric explosions. To test this possibility, the present results are compared with LS atmospheric explosions, conducted by Shell Research Ltd. in a large steel box (L × W × H = 10 m × 8.75 m × 6.25 m) [28] and by FM Global [29] in a 64 m$^3$ vented enclosure (L × W × H = 4.6 m × 4.6 m × 3.0 m), with a single 5.4 m$^2$ vent to keep the internal pressure constant during flame propagation. Comprehensive correlating equations of the pressure effects on the onset of instability, as well as those of Markstein numbers, have been developed and presented at various experimental conditions.

The flame stretching arising from the flow field, together with the effects of thermo-diffusion can stabilize, or further destabilize the potential instabilities in explosions. In the early stage of a flame propagation, the flame is subjected to a high rate of stretch due to the relatively small flame surface area and amplification caused by residual spark energy. This high stretch level helps smooth the wrinkling of the flame surface up to a critical radius, $r_{cl}$, at which the stretch is no longer sufficient to stabilize the smooth structure of the flame [30]. Beyond $r_{cl}$, the Darrieus-Landau (D-L) and thermo-diffusive instabilities produce a strong wrinkling on the flame surface, which leads to an increase in the flame speed and an amplification in the pressure pulse [21]. Severe problems were encountered in attempts to model this phenomena mathematically, and solutions have only been possible for a small flame radius of a few centimeters. As a result, several researches have employed a combination of fractal analyses [27,28] and experiments [29,30] on LS explosions with flame radii of several meters [4,31]. Derek et al. [21] studied the large

scale explosion of hydrocarbon fuels and proposed $K_{cl}$-$Ma_{sr}$ correlations for predicting the stable regime of large scale flames. It is worth recalling that, firstly, the existing correlations do not account for hydrogen components that feature fast burning and enhance the proneness of flame instability when adding to methane-air mixtures; secondly, that the pressure effect on magnifying flame instability is missed out. Available experimental data are scarce for large-scale hydrogen flames. It is therefore necessary to revisit the hydrogen flames in a timely manner given the potential of hydrogen to replace hydrocarbons derived from natural gas and crude oil.

Thermal-diffusive instability can neutralize or delay the onset of D-L instability. The combined effects have been studied by Clavin [32] and, with particular reference to spherical explosion flames, by Bechtold and Matalon [33], who introduced critical values of Peclet number, $Pe_{cl}$ ($= r_{cl}/\delta_l$), for the onset of the flame instabilities. Where $r_{cl}$ is the critical flame radius, defined at which $S_n$ suddenly deviates from its prior response to the stretch rate, and $\delta_l$ is the flame thickness [34]:

$$\delta_l = \frac{(k/c_p)_{T^o}}{\rho_u u_l} \tag{1}$$

where $(k/c_p)_{T^o}$ is the ratio of thermal conductivity to mass-based specific heat, calculated at a given temperature, $T^o$. In hydrogen flames, H radicals diffuse far upstream of the reaction layer, where they are created, and reunite there. Therefore, the preheat zone is not chemically inert for such flames. For such reason, Göttgens et al. [34] and Palacios & Bradley [35] showed that the above expression is more suitable for calculating the thickness of $H_2$ flames, than many other expressions, as the basic assumption of a chemically inert preheat zone is not valid for $H_2$ flames. Equation (1) is employed in the present work as it determines a thickness of a layer, which is defined by the location of a temperature, $T^o$, below which there is no reaction. Bechtold and Matalon demonstrated how spherical flames can be unstable to both types of instability between inner and outer wavelength limits, or cut-offs. These limits of the growth of the perturbation in terms of a wave number, $n$, given by Ref. [26]:

$$n = 2\pi Pe/\Lambda \tag{2}$$

where $Pe$ is the general Peclet number and $\Lambda$ the wavelength, normalized by $\delta_l$. This wavenumber indicates the number of wavelengths of a given value around the circumference of the flame. The higher the value of $n$ is, the greater is the potential number of cells on the flame surface [26,28]. At $Pe_{cl}$, instabilities are initiated at the longest wavelengths associated with a limiting lowest unstable wave number. Before the critical Peclet number, $Pe_{cl}$, is attained (i.e $Pe < Pe_{cl}$), the spherical flame is stable, with a laminar burning velocity, $u_n$ , given by:

$$(u_l - u_n)/u_l = KMa_b \tag{3}$$

where $u_l$ is the unstretched burning velocity and $u_n$ is the stretched burning velocity at a given stretch rate. The Karlovitz stretch factor, $K$, is the stretch rate, normalized by the chemical time, $\delta_l/u_l$. When the flame speed Markstein length, $L_b$, is normalized by $\delta_l$, it gives the flame speed Markstein number, $Ma_b$, and the product of $K$ and $Ma_b$ represents the deficit caused by the flame stretch rate in the normalized burning velocity. The effects of thermo-diffusion and activation energy, together with the density ratio through the flame, are, all embodied in the flame speed Markstein number [36]. Because a flame need a sufficiently high stretch rate to be stable, a critical Karlovitz stretch factor, $K_{cl}$, is a more rational theoretical criterion for the onset of instability than $Pe_{cl}$. For a spherical premixed laminar explosion, the relationship between $Pe_{cl}$ and $K_{cl}$ is expressed as [37]:

$$K_{cl} = (2\sigma/Pe_{cl})[1 + 2Ma_b/Pe_{cl}]^{-1} \tag{4}$$

At $K < K_{cl}$, the flame is unstable. Experimental [28,36] and theoretical [27,32] studies have demonstrated the high level of dependency of $K_{cl}$ upon strain rate Markstein number, $Ma_{sr}$.

The present paper reports values of $K_{cl}$ and $Pe_{cl}$ for methane and methane–hydrogen (20%, 40%, 60, 80 and 100% hydrogen by volume) mixtures in spherical explosions, at various equivalence ratios, $\varphi$, and pressures of 0.1, 0.5, and 1.0 MPa. These data were excluded from Ref. [26] because of their wide divergence from the other hydrocarbon data. In the present paper, the results are presented first by $Pe_{cl}$ as a function of $Ma_b$ then, by $K_{cl}$ as a function of $Ma_{sr}$. A multiple regression method [36] was employed to obtained, $Ma_{sr}$, by determining the strain rate Markstein length, $L_{sr}$, from $u_n$, and the associated flame stretch rate, $\alpha_{sr}$, using. $L_{sr}$ is then normalized by $\delta_l$, to yield $Ma_{sr}$.

Values of $K_{cl}$ and $Ma_{sr}$ are also measured for different $CH_4$/$H_2$ mixtures at pressures higher than atmospheric pressure, where the reduced value of $\delta_l$ resulted in higher values of Peclet number and lower values of $K_{cl}$. Such large values of $Pe$ and small $K_{cl}$ also arise in large atmospheric explosions. These values are compared with some experimental data, which have been drawn from large atmospheric explosions. The results suggest that experimental data on the onset of instabilities, at high pressures, in small scale combustion vessel, can be used to predict those in LS atmospheric explosions. As a main novelty of the present correlations, both pressure effect and hydrogen addition effect that influence the proneness of flame instability have been carefully studied and taken into account.

## Methodology

Measurements were conducted in a spherical stainless steel fan-stirred combustion vessel, with an inner diameter of 380 mm. Fig. 1 shows schematic of the vessel and its auxiliary systems. This vessel was designed to be able to withstand an initial pressure of 1.5 MPa (for hours) and an instantaneous pressure rise up to 9 MPa (for milliseconds). A static pressure transducer (Druck PDCR 911), with a range of 0–1.5 MPa was connected to an LCD display, employed to measure absolute pressure in the vessel during the mixture preparation. Prior to triggering an explosion, a swage lock ball valve was used to isolate this transducer from the rapid pressure rises experienced during explosions. The dynamic pressure was measured by a piezoelectric dynamic pressure transducer

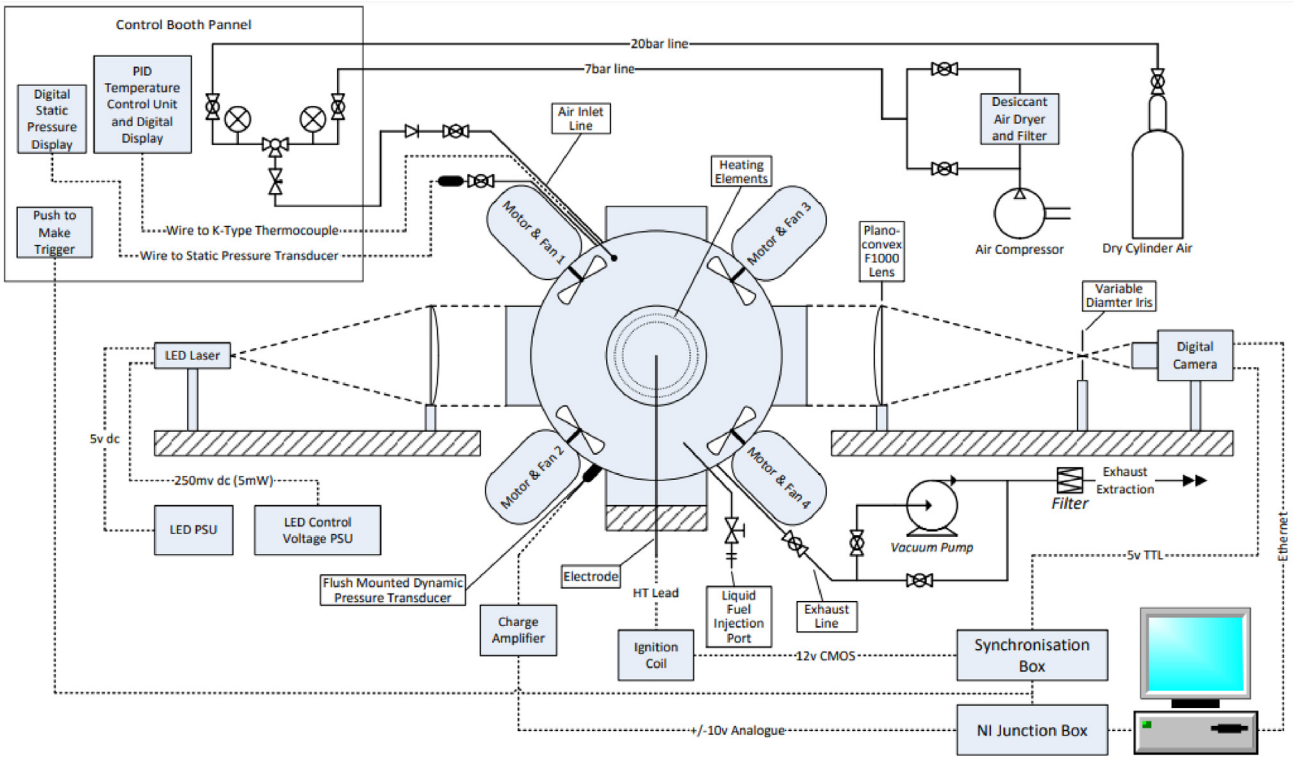


**Fig. 1 – Schematic of the vessel and its auxiliary systems.**

(Kistler 701 A), with a range of 0–25 MPa, mounted flush to the inner wall of the vessel. The output charge from this transducer was converted to an analogue signal of (0–10 V) by a Kistler 5007 charge amplifier. To maximise the signal to noise ratio, the charge amplifier range was set at 0.5 v/MPa. An analogue to digital convertor (Microlink 4000), digitised this voltage signal, which was then interpreted by a LabVIEW software. The vessel was fitted with three pairs of optically windows of 150 mm diameter, to allow a full visualization of the centre of the vessel and the development of instability in the form of the formation of cusps due to the contraction of concave parts of the flame front and cells of smaller wavelength limited by cracks. Four identical fans were mounted close to the inner wall of the vessel. In the present work, those fans were used to ensure that the reactants were well mixed. They are also used during the heating, to generate a turbulent flow which aid in enhancing the convective heat process and spread the heat uniformly throughout the vessel. The fans were switched off prior to ignition and a 15s time period was allowed, to ensure a full decay of turbulence and allow the mixture to equilibrate and become quiescent. During the mixture preparation, the initial temperature was measured by a 25 μm Chromel-Alumel wire Type K thermocouple, sheathed in a 1.5 mm diameter stainless steel tube and positioned 75 mm away from the vessel inner surface, to avoid any radiation and conduction effects from the vessel wall.

High-speed Schlieren cine' photography was installed, as shown in Fig. 1, and employed to capture flame images, from which laminar flame speeds, $S_n$, and critical flame radius, $r_{cl}$, were derived. Depending on the flame speed of the mixture, various resolutions and frame rates was employed. At 0.1 MPa, the camera frame rate and resolution were 20,000 fps and 768 × 768 pixels, respectively, with a pixel size of 0.195 mm/pixel. At 0.5 and 1.0 MPa, the camera frame rate was increased to 30,000 fps and the resolution was reduced to 512 × 512 pixels, with a pixel size of 0.27 mm/pixel.

Combustible methane and methane–hydrogen (20%, 40%, 60, 80 and 100% hydrogen by volume) mixture quantities were prepared in the vessel, with gas concentrations calculated based on partial pressures. The percentage of hydrogen, based on volume, in the fuel blends ($X_{H2}$) was calculated as, $X_{H_2} = V_{H_2}/(V_{CH_4}+V_{H_2})$, where $V_{CH4}$ and $V_{H2}$ are the methane and hydrogen fractions in the fuel blends, respectively. Purities of hydrogen and methane were 99.99% and 99.95%, respectively. Experiments were conducted at initial pressures of 0.1, 0.5 and 1.0 MPa, over a wide range of equivalence ratios. The total equivalence ratio ($\varphi$) was defined as:

$$\varphi = \frac{F/A}{(F/A)_{st}} \tag{5}$$

where $(F/A)$ is the fuel to air ratio and its stoichiometric value is $(F/A)_{st}$. For methane/hydrogen/air mixtures, the chemical combustion formulas can be expressed as:

$$(1-X_{H_2})CH_4 + X_{H_2}H_2 + \left(\frac{2}{\varphi}(1-X_{H_2})\frac{X_{H_2}}{2\varphi}\right)(O_2+3.76N_2) \tag{6}$$

Because the combustion contains three reactants (i.e. methane, hydrogen and air), the stoichiometric parameters must be first defined for data reduction. The mole fractions of methane, hydrogen, methane/hydrogen blend and air are defined as $n_{CH_4}$, $n_{H_2}$, $n_{fuel}$ and $n_{air}$, respectively. The methane and hydrogen based equivalence ratios are then expressed as:

$$\varphi_{CH_4} = \frac{n_{CH_4}/n_{air}}{(n_{fuel}/n_{air})_{st}} \quad (7)$$

$$\varphi_{H_2} = \frac{n_{H_2}/n_{air}}{(n_{fuel}/n_{air})_{st}} \quad (8)$$

where the denominator of $\varphi_{CH_4}$ and $\varphi_{H_2}$ is the stoichiometric F/A stoichiometric in a molar basis, and the numerator is the ratio of individual fuel (i.e. methane or hydrogen) to the amount of air, required for its oxidation.

In present work, since there are two fuels in the mixture, the Lewis number is calculated and presented as an average value, as [38]:

$$Le_{eff} = 1 + \frac{q_{CH_4}(Le_{CH_4} - 1) + q_{H_2}(Le_{H_2} - 1)}{q} \quad (9)$$

where $q_{CH_4}$ and $q_{H_2}$ are the non-dimensional heat release associated with the consumption of $CH_4$ and $H_2$, respectively, and $q$ is the total heat release ($q = q_{CH_4} + q_{H_2}$). The values of $q_{CH_4}$ and $q_{H_2}$ can be obtained from: $q_{CH_4} = QY_{CH_4}/C_pT_u$ and $q_{H_2} = QY_{H_2}/C_pT_u$, respectively. Here, Q is the heat of reaction, $C_p$ is the specific heat at constant pressure, $T_u$ is the unburned gas temperature. $Y_{CH_4}$ and $Y_{H_2}$ are the supply mass fractions of $CH_4$ and $H_2$, respectively. Fig. 2 shows Lewis number for all mixtures, at different pressures.

The initial temperature was kept 300 K for all experiments. To ensure no residual gases from successive explosions in the vessel, the vessel was evacuated at least two times down to 0.0015 MPa, after each test. Dry air was used to prepare the combustible mixture. A conventional automotive spark plug, supplying about 23 mJ, was employed to initiate the ignition of mixtures at the centre of the vessel. Further details of the vessel are available in Refs. [39,40].

The onset of Darrieus–Landau, thermo-diffusive instabilities was defined from the rapid deviation of flame speed, $S_n$, from its prior response to stretch rate. The flame speed, $S_n$, was calculated from the temporal evolution of flame front radius, $r_u$, as $S_n = dr_u/dt$. The overall stretch rate, $\alpha$, of a spherical expanding flame is given by $\alpha = (2/r_u)(dr_u/dt)$. The linear dependency of $S_n$ on $\alpha$ allowed $u_l$ and $L_b$ to be estimated from:

$$S_s - S_n = L_b\alpha \quad (10)$$

where $S_s$ is the unstretched flame speed, and is obtained as the intercept value of $S_n$ at $\alpha = 0$, in the plot of $S_n$ against $\alpha$. The Markstein length, $L_b$, is the gradient of $S_n$-$\alpha$ curve, which is measured in the stable regime, between the radius beyond which there is no effect of the spark plasma and the onset of instabilities. As $\varphi$ an $P$ increase, this stable system gradually becomes restricted. The unstretched laminar burning velocity, $u_l$, is derived from $S_s$ by dividing this value by the unburned to burned gas density ratio, $\sigma$. Values of $\sigma$ are obtained from Gaseq [41], at the unburned gas temperature.

The critical radius, $r_{cl}$ , was measured from the plots of $S_n$ against $\alpha$, at which $S_n$ suddenly increases. It represents the transition from a smooth laminar flame front to a fully cellular flame. The values of $r_{cl}$, $L_b$ and $L_{sr}$, were normalized by $\delta_l$, to yield $Pe_{cl}$, $Ma_b$ and $Ma_{sr}$, respectively.

## Results and discussion

### Flame speeds

Variation in the stretched flame speed, $Sn$, with flame radius, obtained from the temporal evolution of the flame front, (i.e. $S_n = dr_u/dt$) for explosions of (60% $H_2$+ 40% $CH_4$) at $\varphi = 0.8$, and pressures of 0.1, 0.5 and 1.0 MPa is shown in Fig. 1. A single representative explosion was chosen of three experiments performed at each condition. Fig. 2 shows a similar relationships for $\varphi = 1.2$. All flame speeds in Figs. 3 and 4 are initially extremely high and decreases to a lower values. These high values are the result of the initiating spark plasma being sufficiently high to over-drive the flame. This is a well-known experimental phenomenon [42]. The limit for the onset of the stable regime can be identified from plots of both $Sn$ against $r_u$,

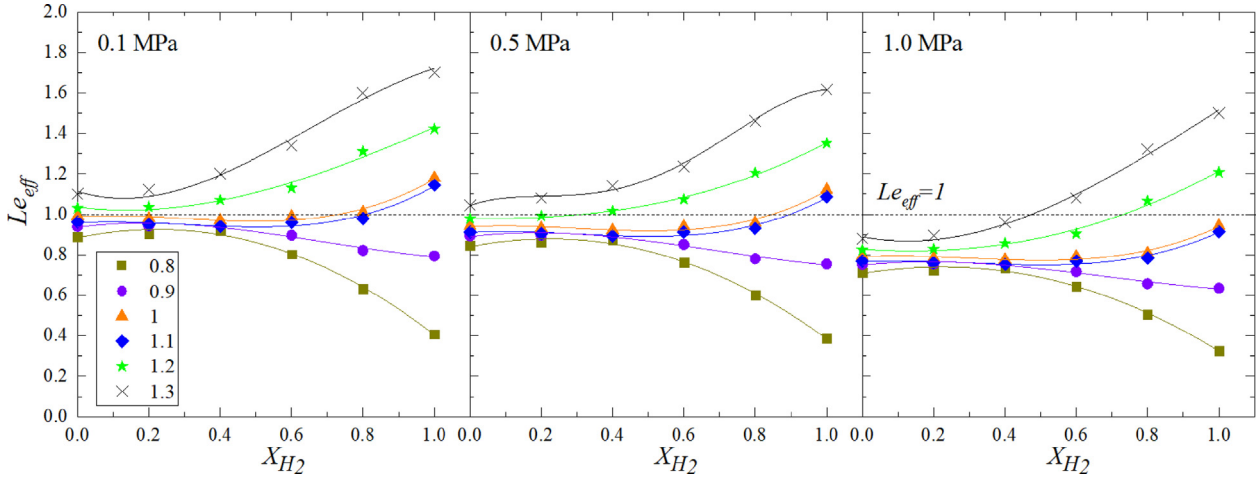


**Fig. 2 – The effective Lewis number plotted against hydrogen fraction, $X_{H_2}$, for various equivalence ratios at P = 0.1, 0.5 and 1.0 MPa.**

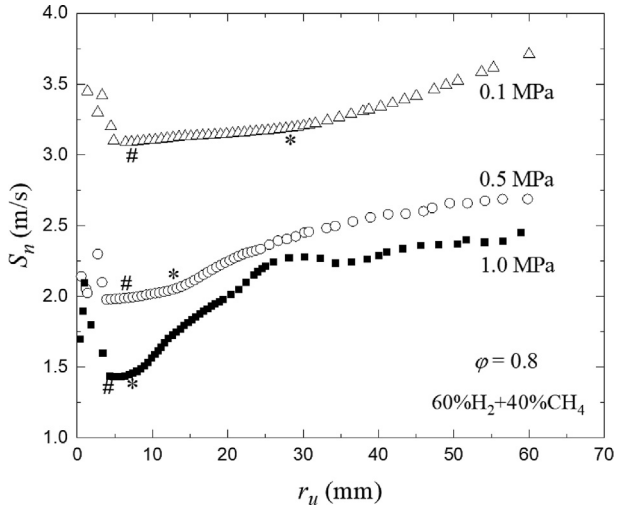


**Fig. 3 – Variations of $S_n$, with $r_u$, for (60% $H_2$+ 40% $CH_4$) mixture at $\varphi = 0.8$, and pressures of 0.1, 0.5 and 1.0 MPa.**

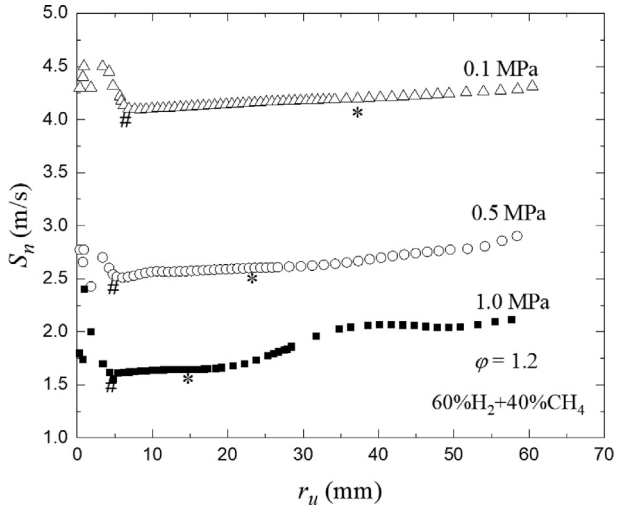


**Fig. 4 – Variations of $S_n$, with $r_u$, for (60% $H_2$+ 40% $CH_4$) mixture at $\varphi = 1.2$, and pressures of 0.1, 0.5 and 1.0 MPa.**

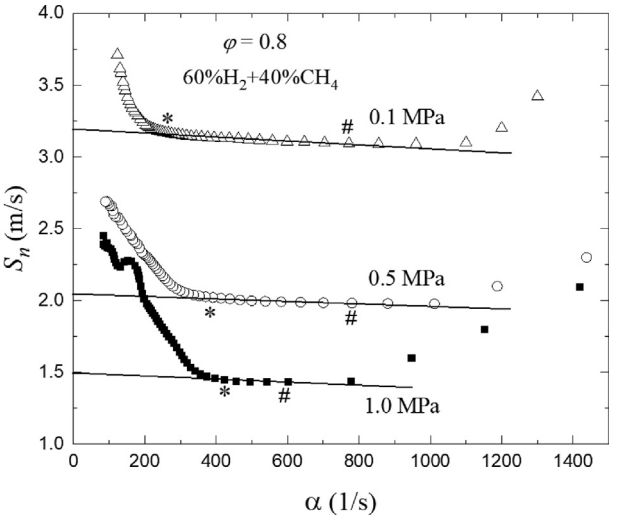


**Fig. 5 – Variations of $S_n$, with $\alpha$, for (60% $H_2$+ 40% $CH_4$) mixture at $\varphi = 0.8$, and pressures of 0.1, 0.5 and 1.0 MPa.**

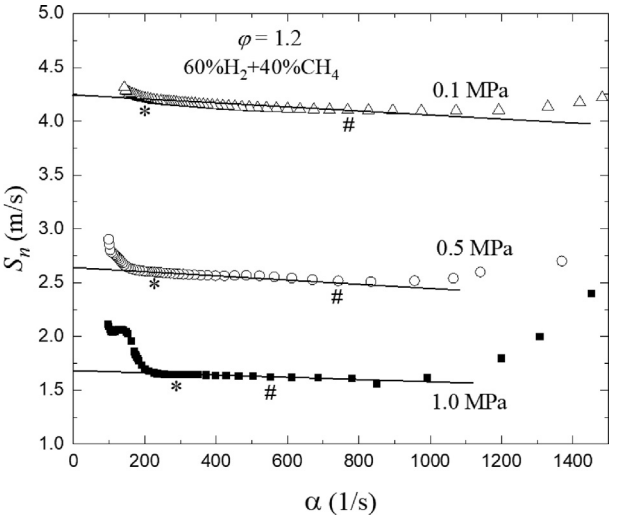


**Fig. 6 – Variations of $S_n$, with $\alpha$, for (60% $H_2$+ 40% $CH_4$) mixture at $\varphi = 1.2$, and pressures of 0.1, 0.5 and 1.0 MPa.**

as in Figs. 3 and 4, and, even more appropriately, from plots of *Sn* against $\alpha$, as in Figs. 5 and 6 for the same conditions. In these figures the inner limit, beyond which there is no effect of the spark plasma, is indicated by (#). The instability effect became considerably high at high pressure, as shown from Figs. 3 and 4, where the critical radius is indicated by, *, for all $\varphi$. In all cases, as pressure increases, the stable regime in which the burned Markstein length, $L_b$ , can accurately be measured becomes increasingly limited, between the minimum unaffected spark radius of about 6 mm [36] and the onset of cellularity, at the critical radius, *rcl*. Simulations for H2/air flames in Ref. [19] showed the inner limit to increase with increase in Lewis number. Similar effect can be observed for (60% $H_2$+ 40% $CH_4$) in Figs. 5 and 6, where the latter, for $\varphi = 1.2$, has a higher values of Lewis number (Fig. 2), and smaller values of stretch rates at the # points. With increasing the initial pressure, the thermo-diffusive effect on destabilizing flames is minimal, as the effective *Le* is insensitive to changes in pressure as shown in Fig. 2. Since the thermal expansion keeps almost the same value, whereas, the flame thickness decreases significantly with increasing the initial pressure, this sudden increase in velocity, in Figs. 5 and 6, can only be attributed to the hydrodynamic instability. Kwon et al. [43] have shown that thinner flames reduces the effect of curvature and increases the baroclinic intensity, which increases the hydrodynamic instability. From the plots of $S_n - \alpha$, using linear extrapolation within the stable regime of the flame, values of unstretched flame speed, *Ss*, were obtained, from which the unstretched laminar burning velocity, $u_l$, was calculated, using $u_l = (\rho_b/\rho_u)S_s$, and the flame speed Markstein length, $L_b$ , was found using Eq. (10). This length was normalized by the flame thickness to obtain the burned Markstein number, $Ma_b$.

Changes in the stretched flame speed, $S_n$, with flame stretch rate, $\alpha$, for mixtures with hydrogen fractions ($X_{H2} = 0\%$,

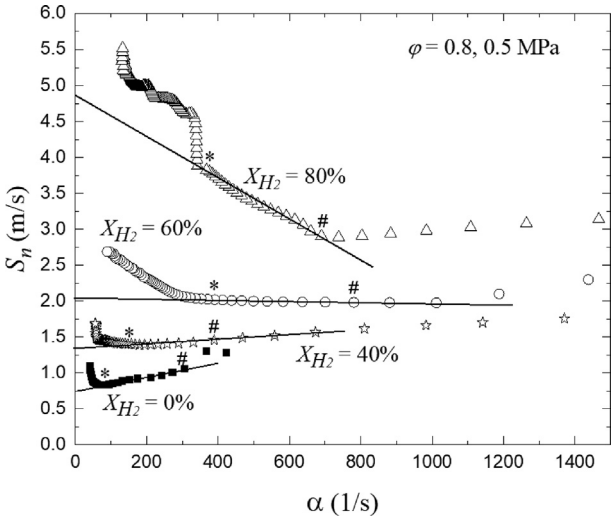


**Fig. 7 – Variations of $S_n$, with $\alpha$, at different initial pressures for $CH_4/H_2$/air mixtures.**

40%, 60% and 80%) are shown in Fig. 7, at $\varphi = 0.8$ and P = 0.5 MPa. As hydrogen fraction increases, so does the flame speed. The flame instability also increases with increasing the hydrogen fraction, which can be attributed to the lower Lewis number at high hydrogen fraction (Fig. 2). The burned gas Markstein lengths, $L_b$, decreases with increasing the hydrogen fraction, which indicates that the flame instability increases with the increase of $H_2$ fraction in the mixture.

### *Critical peclet number*

Experimental values of $Pe_{cl}$ for $CH_4$/air at a temperature of 300 K and pressures of 0.5, 1.0 MPa, are plotted against measured values of $Ma_b$ in Fig. 8. Each experimental point is an average of three explosions. The onset of instability in $CH_4$ explosions is not observed at 0.1 MPa, where flames

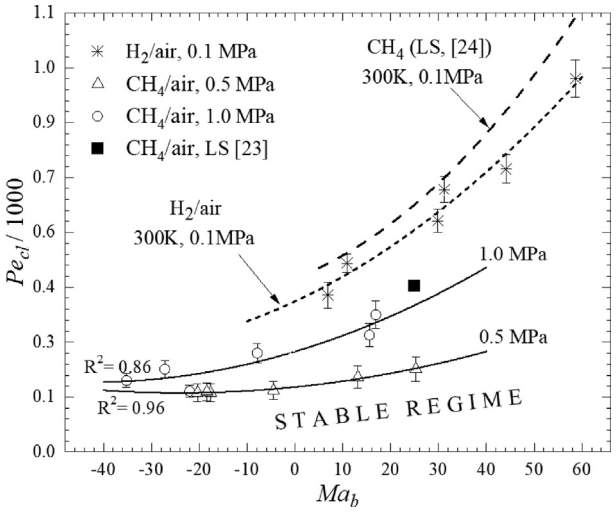


**Fig. 8 – Variation of $Pe_{cl}$ with $Ma_b$ for $CH_4$ and $H_2$ at different pressures in the laboratory combustion vessel, with data from LS explosions at atmospheric conditions [23,24].**

remained stable within the visualization measurement area (R = 75 mm). The values of $Pe_{cl}$ increase with increasing pressure, P, due to the decreasing flame thickness, indicating that the increase in P promotes the hydrodynamic instability. The dotted line gives the experimental values of $H_2$/air at 300 K and 0.1 MPa. At 0.5 and 1.0 MPa, accurate measurement of $L_b$ for pure $H_2$/air, and hence $Ma_b$, become extremely challenging due to the very short time interval between the end of sparking and the onset of cellularity. The flames became cellular almost immediately after being established. Consequently, results at high pressures for pure $H_2$/air are not presented here. The dashed line represents data from LS explosions at atmospheric conditions [23,24], values of $Pe_{cl}$ have been measured for, LS, $CH_4$/air by the Factory Mutual group. Flames are measured up to a diameter of 2 m, with $\varphi$ varied between 0.81 and 1.22. These values are plotted against values of flame speed Markstein numbers, from Ref. [44]. The bold black square is a data point for $CH_4$/air from LS explosions at atmospheric conditions, conducted by Shell Research Ltd. in a large vented steel box (L × W × H = 10 m × 8.75 m × 6.25 m) [23]. For all cases, flames with higher values of $Ma_b$ have a higher $Pe_{cl}$. The values of pure $H_2$/air flames are close to those of LS $CH_4$/air at 0.1 MPa. The difference between Shell and Factory Mutual LS data are attributable to the different methods of deriving $Ma_b$. Errors in $Ma_b$ are also significant [44], especially at negative values of $Ma_b$, due to the short duration of the stable regime [30], and extrapolation to zero stretch rate may necessitate the use of a fractal expression. More errors might also arise from the different methods in which $r_{cl}$ is defined. Importantly, the two sets of data from the LS explosions at atmospheric conditions are close to those from the small-scale explosions at high-pressure (i.e. 1.0 MPa), and slightly higher at 0.5 MPa. As the pressure increases, $\delta_l$ decreases yielding higher values of $Pe_{cl}$ close to those of the atmospheric explosions with higher radii.

### *Effects of pressure and hydrogen content on critical peclet number $Pe_{cl}$*

Fig. 9 shows the development of stoichiometric spherically expanding $H_2$/air flames at 0.1 and 0.5 MPa. In contrast to the previous studies [38–45] in which no stabilities are reported in pure $H_2$/air explosions at 0.1 MPa, the current Schlieren images show a flame surface with continuous cracking at such pressure. The current vessel and windows are large enough for the development of instabilities to be observed, compared to other vessels with small sizes [38–45]. At 0.1 MPa, the first appearance of cracking can be interpreted as the onset of instability (at $r_{cl}$ = 50.1 mm). At 0.5 MPa, Fig. 9b, a fully developed cellular structure was observed at the early stages of flame propagation (at $r_{cl}$ = 12.1 mm). Clearly, the onset of instabilities occurs at $r_{cl}$ values that decrease with increasing pressure. As the flame grows further, a large number of cells are formed on the flame surface, and flame speed $S_n$ increases significantly. To determine the cause of the tendency to destabilize with increasing pressure, it is recognized that since the composition of the mixture is fixed for given values of $\varphi$ and hydrogen content, and the flame temperature is not quite sensitive to changes in pressure, the thermal expansion

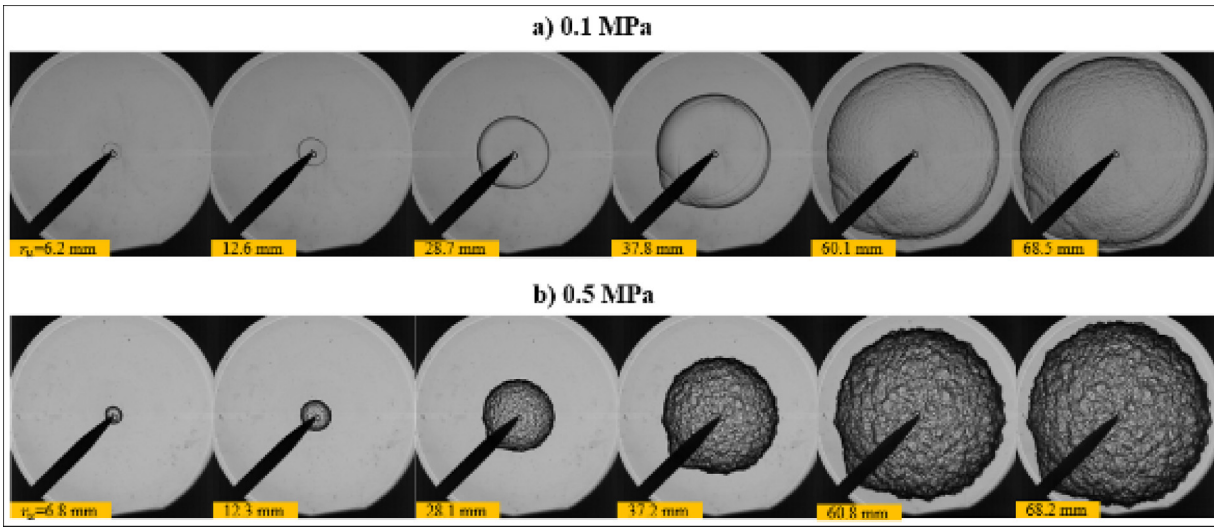


**Fig. 9 – Images of stoichiometric $H_2$/air flames, at (a) 0.1 MPa, and (b) 0.5 MPa.**

ratio, $\sigma = \rho_u/\rho_b$, is approximately the same for the two cases shown in Fig. 9, the remaining parameter that governs the stability is the flame thickness, $\delta_l$. The value of $\delta_l$ clearly shows that the tendency to destabilize increases with decreasing $\delta_l$ and hence with increasing pressure.

Fig. 10 shows the critical flame radius, $r_{cl}$, and the flame thickness, $\delta_l$, as a function of equivalence ratio, $\varphi$, for different values of hydrogen content in the fuel ($X_{H2} = 0.2$; 0.4; 0.6; 0.8 and 1.0) at 0.1 MPa. The onset of instability is noticed at an early stage for pure $H_2$ ($X_{H2} = 1$), and no instability is observed for pure $CH_4$ ($X_{H2} = 0$). As $\varphi$ increases, from lean to rich, the flame gradually becomes more stable. Since the composition of mixtures is fixed for given values of $\varphi$ and $X_{H2}$, the parameter that governs the flame stability is the thickness, $\delta_l$. Fig. 10 demonstrates that the propensity to increases with decreasing $\delta_l$, in addition to the influence of the Lewis number which increase with the increase of the hydrogen content [46], indicative of a more stable flame.

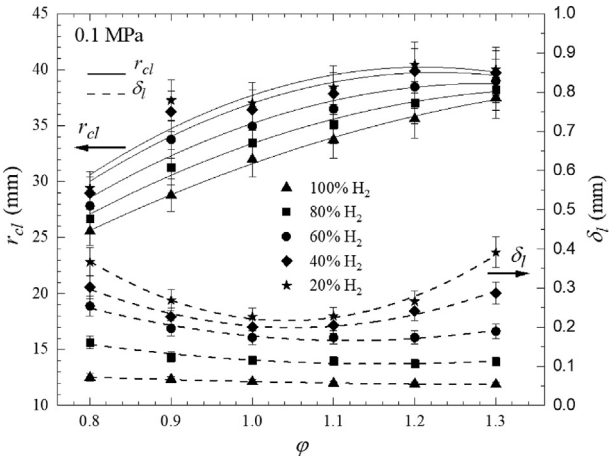


**Fig. 10 – Critical radius (solid lines) for onset of instability from experiments, and calculated flame thickness (dashed lines), both as a function of $\varphi$ for different values of hydrogen content, at 0.1 MPa.**

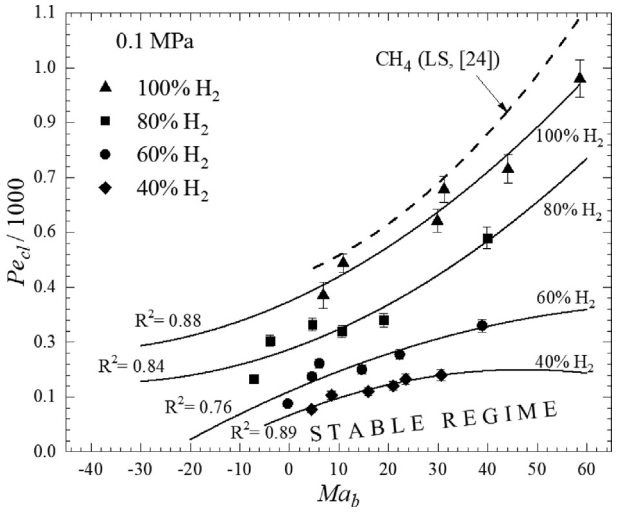


**Fig. 11 – Variation of $Pe_{cl}$ with $Ma_b$ for different values of $H_2$ content, at 0.1 MPa. Dashed line represents data from large-scale explosions [24].**

Values of $Pe_{cl}$ for different values of hydrogen content in the fuel ($X_{H2} = 0.4$; 0.6; 0.8 and 1.0) versus $Ma_b$ at 0.1 MPa and 300 K is shown in Fig. 11. For a given $Ma_b$, $Pe_{cl}$ increases, and hence the flame becomes progressively more stable, with the increase of hydrogen fraction. This stabilizing result is supported by the decreasing flame thickness with the increase of $X_{H2}$, Fig. 10. $Pe_{cl}$ increases with the increase of $Ma_b$ up to $X_{H2} = 0.6$, and becomes nearly constant for large positive values of $Ma_b$( >40). This parabolic-like behavior of $Pe_{cl}$, for low hydrogen content flames, is reasonable because the flame thickness has its minimum values around stoichiometry for these flames. In contrast to $CH_4$/$H_2$/air flames with large hydrogen content (>0.8), $Pe_{cl}$ increases as $Ma_b$ increases. This is attributed to the increase of both the laminar burning velocity and the maximum concentration of hydrogen atoms, compared those of pure $CH_4$/air and low $H_2$ fractions flames. The high burning velocity of $H_2$/air premixed flames can be

attributed to the rapid exothermic reactions in the lower temperature flame regions which require diffusion-promoted hydrogen atoms from the flame front according to the diffusion mechanism of these flames, which increases the flame instability. In contrast, $CH_4$/air premixed flames propagate due to the thermal energy transported by conduction from high temperature regions to low temperature regions, hence these flames have much lower speeds and they are more stable.

### *Critical karlovitz number*

The dimensionless Karlovitz flame stretch factor, K, was usually used to quantify flame straining [26]. Hence, appropriate laminar flame analyses of the effects of flame stretch rate suggests both $Ma_{sr}$ and $K$, as correlating parameters. Fig. 12 shows $K_{cl}$ for $CH_4$/air, derived from Eq. (4), by the bold symbols for various values of $Ma_{sr}$ , at 0.5 and 1.0 MPa. Also shown by the dashed curve are LS data for the same fuel, taken from Ref. [24] at atmospheric conditions. Best-fit curves of the present experimental data are shown for such high pressures explosions (at 0.5 and 1.0 MPa). All curves exhibit the same trend of more significant decreases in $K_{cl}$ as $Ma_{sr}$ increases. Increasing the pressure from 0.5 MPa to 1.0 MPa leads to a decrease in $K_{cl}$, indicative of generally increased flame instability. The effect of pressure can be generalized to give a formula for $K_{cl}$ in terms of $P/P_a$ and $Ma_{sr}$ :

$$K_{cl} = 0.0067 \exp(-0.063 Ma_{sr})(P/P_a)^{-0.81} \quad (11)$$

Increasing the pressure reduced the flame thickness, which in turn yielded lower values of Karlovitz number, simulating atmospheric explosions with higher radii. Based on this theory, equation (11) was derived using the experimental data in Fig. 12. The critical Karlovitz number was first calculated form Small-Scale explosions at 0.5 MPa and 1.0 MPa in our vessel and from Large-Scale explosions at 0.1 MPa, taken from Ref. [24]. The results were plotted against values of strain-rate Markstein numbers. The best-fit exponential curve, which fits with the three curves in Fig. 12 and gives the highest possible $R^2 = 0.88$, was obtained and extrapolated to fit all points of the large-scale explosion data from LS [24]. Only one curve can fit all points and hence only one value of P can be obtained. By solving the equation of the extrapolated curve, at LS data, it gives a pressure of $1.9 \pm 0.01$ MPa. The large-scale explosion data from LS [24], is in a fairly close agreement with this expression at $P = 1.9MPa$, which proves that small-scale laboratory experiments at high pressure can provide a solid idea of the onset of instabilities in LS explosions at atmospheric conditions.

All data for $CH_4/H_2$/air are plotted in terms of $K_{cl}$ versus $Ma_{sr}$, at pressures of 0.1, 0.5 and 1.0 MPa in Fig. 13. For $X_{H2} = 0.4$, in Fig. 13a, the increase in pressure exhibits lower values of $K_{cl}$ for all given values of $Ma_{sr}$. Such results show that the flame is tending to be thinner, and the propagation dynamics are dominated by hydrodynamic instability, leading the flame to become unstable due to the decrease in the flame thickness with increasing P. Similar trends are observed for all other $CH_4/H_2$/air mixtures, with increasing $X_{H2}$. At 1.0 MPa, in Fig. 13c, only two data points could be obtained because the time span of stable flame regime became increasingly small with increasing P. For pure $H_2$/air in Fig. 13d, no data was obtained at 1.0 MPa, and only two data points were obtained

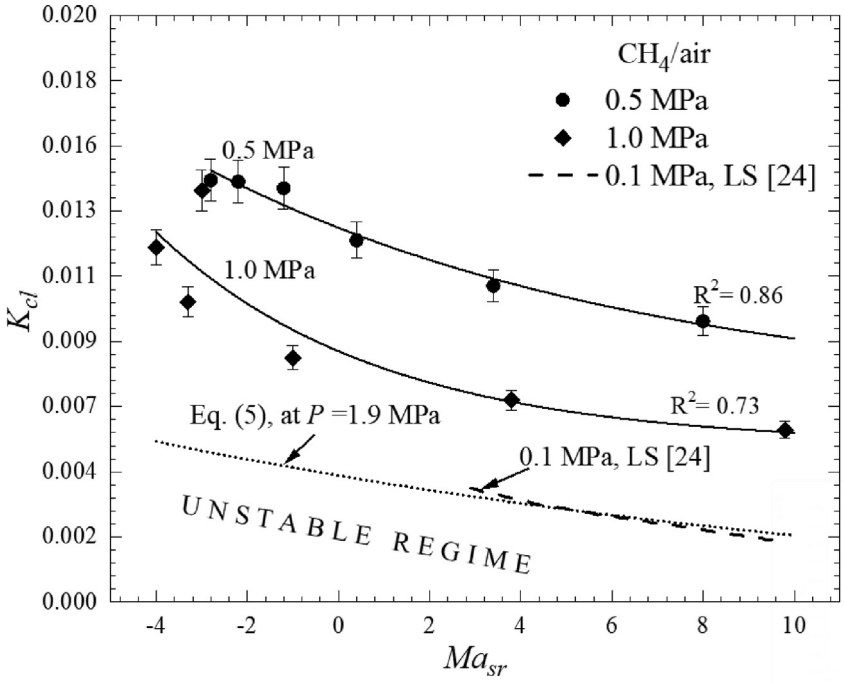


**Fig. 12 – Variation of $K_{cl}$ with $Ma_{sr}$ for pure $CH_4$/air explosion vessel data, at different pressures. Filled circles (0.5 MPa), filled rhombus (1.0 MPa). Solid curves shows the best fits through the experimental data. Dashed line is data from large-scale explosions [24], at 0.1 MPa.**

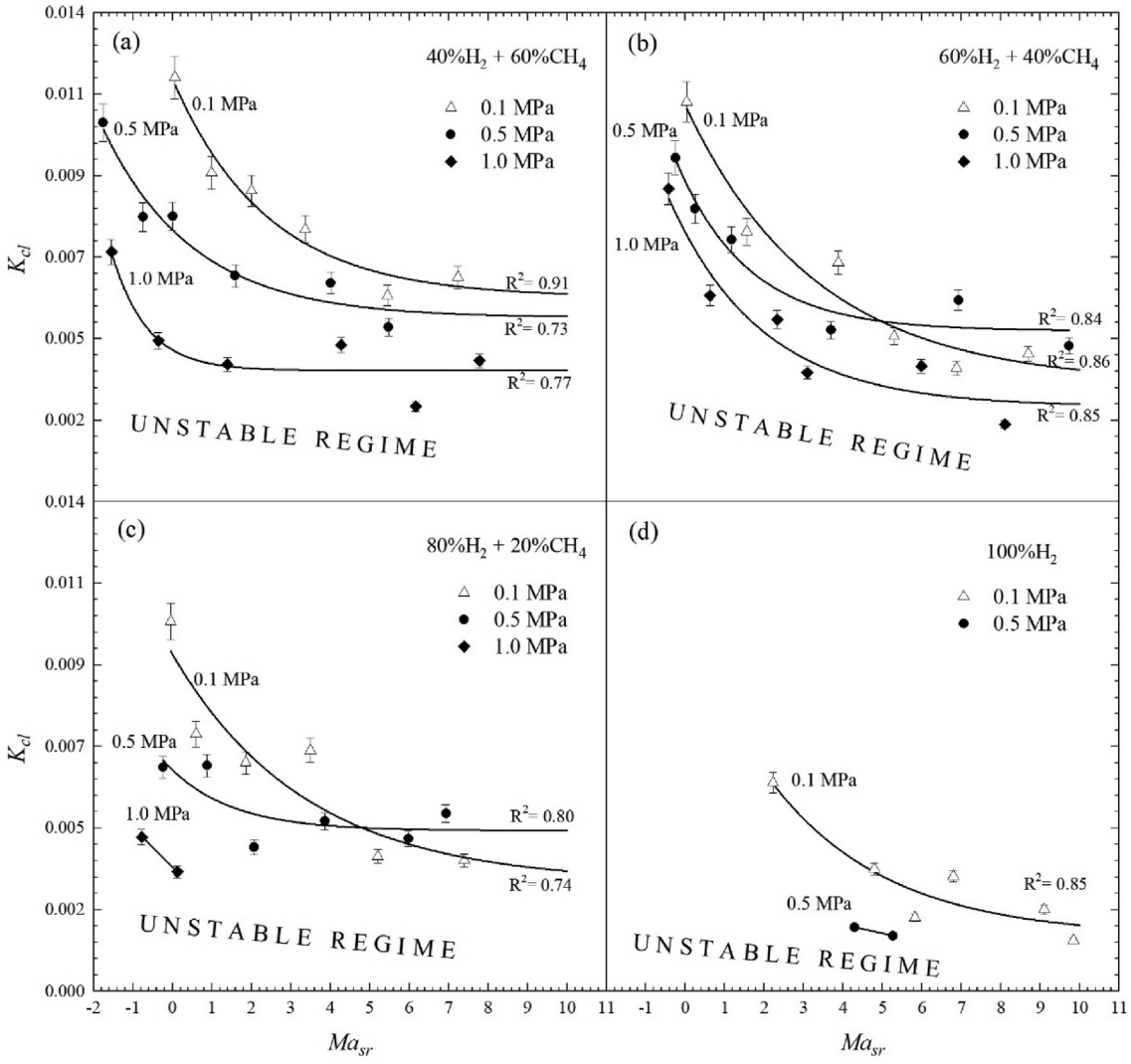


**Fig. 13 – Values of $K_{cl}$ plotted against $Ma_{sr}$ for $CH_4/H_2$/air flames with ($X_{H2} = 0.4$; 0.6; 0.8 and 1.0), at different pressures. Open tringles (0.1 MPa), filled circles (0.5 MPa), filled rhombus (1.0 MPa). Solid curves shows best fits through the experimental data.**

for 0.5 MPa. The results in Figs. 12 and 13 can be empirically correlated at different pressures using the following expressions:

$$K_{cl} = (0.0136 - 0.0077X_{H_2})\exp(-0.093X_{H_2} - 0.062)Ma_{sr} \quad \text{at 0.1 MPa, } R^2 = 0.85 \tag{12}$$

$$K_{cl} = (0.0154 - 0.0089X_{H_2})\exp(-0.0621X_{H_2} - 0.0613)Ma_{sr} \quad \text{at 0.5MPa, } R^2 = 0.67 \tag{13}$$

$$K_{cl} = (0.0081 - 0.0075X_{H_2})\exp(-0.01X_{H_2} - 0.0581)Ma_{sr} \quad \text{at 1.0 MPa, } R^2 = 0.74 \tag{14}$$

where $R^2$ is a statistical measure of how close the data are to the fitted regression curve. Regardless of the scatter, increasing pressure led to a definite tendency for a smaller $K_{cl}$ and more unstable flames. Such values of $K_{cl}$ provide datums below which the large scale flame becomes unstable.

The important role of $K_{cl}$ as well as the small values of $\delta_l$, that can be obtained in high pressure small-scale explosions, allowed the onset of instabilities in LS explosions at atmospheric pressure, $P_a$ , to be predicated from those small-scale laboratory explosions. Figs. 12 and 13 clearly show the influences of hydrogen content, through values of $Ma_{sr}$, and pressure upon $K_{cl}$, and hence $Pe_{cl}$. These effects can be generalized to give an expression for $Pe_{cl}$ in terms of different values of $(P/P_a)$ and $Ma_{sr}$. For all $CH_4/H_2$/air mixtures studied in the explosion vessel, these results can be empirically correlated by:

$$K_{cl} = (0.027 - 0.0041X_{H_2})\exp(-0.0261X_{H_2} - 0.0751)\, Ma_{sr}(P/P_a)^{-0.25} \qquad R^2 = 0.79 \tag{15}$$

## Conclusions

An experimental study on onset of instabilities of methane/hydrogen/air mixtures was conducted in a small-scale constant volume spherical vessel, at different initial pressures and hydrogen fractions. The results were compared with large-scale industrial explosions at atmospheric conditions. The conclusions are summarized as follows.

(i) The results suggest that small-scale laboratory explosions at high pressure (~1.9 MPa), can be employed to predict the onset of instability in LS atmospheric explosions.
(ii) An empirical correlation of $K_{cl}$ as a function of $Ma_{sr}$ and $P/P_a$ is obtained and presented. This equation can be used to predict the onset of instabilities in $CH_4/H_2$/air explosions.
(iii) The critical Peclet number, $Pe_{cl}$, and the critical Karlovitz number, $K_{cl}$, have been presented as a function of the flame speed Markstein number, $Ma_b$, and the strain rate Markstein number, $Ma_{sr}$. Correlations of $K_{cl}$ have been developed at different pressures.
(iv) With the increase of initial pressure and hydrogen fraction, the flame becomes more wrinkled at earlier stage. This indicates that the flame becomes more unstable because of the enhancement of instabilities due to the significant decrease of the flame thickness.
(v) At higher pressure, the repeatability of critical flame radius, $r_{cl}$, became reduced. At 1.0 MPa, accurate measurements for $u_l$ and $L_b$ were only possible for low hydrogen contents (<0.8). Beyond which the onset of instability occurred immediately after the initiating spark, and the stable regime became insufficient to extrapolate from.

## Declaration of competing interest

The authors declare that they have no known competing financial interests or personal relationships that could have appeared to influence the work reported in this paper.

## Acknowledgment

The authors thank EPSRC (Grant No. EP/W002299/1) for the financial support.

## REFERENCES

[1] Matalon M, Bechtold JK. A multi-scale approach to the propagation of non-adiabatic premixed flames. J Eng Math 2009 Apr;63(2):309–26. https://doi.org/10.1007/s10665-008-9228-0.
[2] Wu F, Jomaas G, Law CK. An experimental investigation on self-acceleration of cellular spherical flames. Proc Combust Inst 2013 Jan 1;34(1):937–45. https://doi.org/10.1016/j.proci.2012.05.068.
[3] Kim W, Sato Y, Johzaki T, Endo T, Shimokuri D, Miyoshi A. Experimental study on self-acceleration in expanding spherical hydrogen-air flames. Int J Hydrogen Energy 2018 Jul 5;43(27):12556–64. https://doi.org/10.1016/j.ijhydene.2018.04.153.
[4] Bauwens CR, Bergthorson JM, Dorofeev SB. Experimental study of spherical-flame acceleration mechanisms in large-scale propane–air flames. Proc Combust Inst 2015 Jan 1;35(2):2059–66. https://doi.org/10.1016/j.proci.2014.06.118.
[5] Cai X, Wang J, Zhao H, Zhang M, Huang Z. Flame morphology and self-acceleration of syngas spherically expanding flames. Int J Hydrogen Energy 2018 Sep 6;43(36):17531–41. https://doi.org/10.1016/j.ijhydene.2018.07.140.
[6] Kim W, Imamura T, Mogi T, Dobashi R. Experimental investigation on the onset of cellular instabilities and acceleration of expanding spherical flames. Int J Hydrogen Energy 2017 May 25;42(21):14821–8. https://doi.org/10.1016/j.ijhydene.2017.04.068.
[7] Bradley D, Sheppart CG, Woolley R, Greenhalgh DA, Lockett RD. The development and structure of flame instabilities and cellularity at low Markstein numbers in explosions. Combust Flame 2000 Jul 1;122(1–2):195–209. https://doi.org/10.1016/S0010-2180(00)00113-9.
[8] Okafor EC, Nagano Y, Kitagawa T. Experimental and theoretical analysis of cellular instability in lean H2-CH4-air flames at elevated pressures. Int J Hydrogen Energy 2016 Apr 27;41(15):6581–92. https://doi.org/10.1016/j.ijhydene.2016.02.151.
[9] Katsumi T, Aida T, Aiba K, Kadowaki S. Outward propagation velocity and acceleration characteristics in hydrogen-air deflagration. Int J Hydrogen Energy 2017 Mar 16;42(11):7360–5. https://doi.org/10.1016/j.ijhydene.2016.06.165.
[10] Huang Z, Zhang Y, Wang Q, Wang J, Jiang D, Miao H. Study on flame propagation characteristics of natural gas– hydrogen–air mixtures. Energy Fuels 2006 Nov 15;20(6):2385–90. https://doi.org/10.1021/ef060334v.
[11] Huang Z, Zhang Y, Zeng K, Liu B, Wang Q, Jiang D. Measurements of laminar burning velocities for natural gas–hydrogen–air mixtures. Combust Flame 2006 Jul 1;146(1–2):302–11. https://doi.org/10.1016/j.combustflame.2006.03.003.
[12] Zhao H, Wang J, Bian Z, Cai X, Li X, Huang Z. Onset of cellular instability and self-acceleration propagation of syngas spherically expanding flames at elevated pressures. Int J Hydrogen Energy 2019 Oct 22;44(51):27995–8006. https://doi.org/10.1016/j.ijhydene.2019.09.038.
[13] Hu E, Huang Z, He J, Zheng J, Miao H. Measurements of laminar burning velocities and onset of cellular instabilities of methane–hydrogen–air flames at elevated pressures and temperatures. Int J Hydrogen Energy 2009 Jul 1;34(13):5574–84. https://doi.org/10.1016/j.ijhydene.2009.04.058.
[14] Emami SD, Rajabi M, Hassan CR, Hamid MD, Kasmani RM, Mazangi M. Experimental study on premixed hydrogen/air and hydrogen–methane/air mixtures explosion in 90 degree bend pipeline. Int J Hydrogen Energy 2013 Oct 25;38(32):14115–20. https://doi.org/10.1016/j.ijhydene.2013.08.056.
[15] Ma Q, Zhang Q, Pang L, Huang Y, Chen J. Effects of hydrogen addition on the confined and vented explosion behavior of methane in air. J Loss Prev Process Ind 2014 Jan 1;27:65–73. https://doi.org/10.1016/j.jlp.2013.11.007.
[16] Yu M, Zheng K, Zheng L, Chu T, Guo P. Effects of hydrogen addition on propagation characteristics of premixed methane/air flames. J Loss Prev Process Ind 2015 Mar 1;34:1–9. https://doi.org/10.1016/j.jlp.2015.01.017.

[17] Cammarota F, Di Benedetto A, Di Sarli V, Salzano E, Russo G. Combined effects of initial pressure and turbulence on explosions of hydrogen-enriched methane/air mixtures. J Loss Prev Process Ind 2009 Sep 1;22(5):607–13. https://doi.org/10.1016/j.jlp.2009.05.001.
[18] Salzano E, Cammarota F, Di Benedetto A, Di Sarli V. Explosion behavior of hydrogen–methane/air mixtures. J Loss Prev Process Ind 2012 May 1;25(3):443–7. https://doi.org/10.1016/j.jlp.2011.11.010.
[19] Chen Z, Burke MP, Ju Y. Effects of Lewis number and ignition energy on the determination of laminar flame speed using propagating spherical flames. Proc Combust Inst 2009 Jan 1;32(1):1253–60. https://doi.org/10.1016/j.proci.2008.05.060.
[20] Bradley D, Lawes M, Morsy ME. Combustion-induced turbulent flow fields in premixed flames. Fuel 2021 Apr 15;290:119972. https://doi.org/10.1016/j.fuel.2020.119972.
[21] Liu Z, Unni VR, Chaudhuri S, Sui R, Law CK, Saha A. Self-turbulization in cellularly unstable laminar flames. J Fluid Mech 2021 Jun;917. https://doi.org/10.1017/jfm.2021.330.
[22] Lind CD, Whitson JC. Explosion hazards associated with spills of large quantities of hazardous materials. China Lake, Calif.(USA): Phase II. Final report. Naval Weapons Center; 1977 Nov 1. https://www.osti.gov/biblio/6886892.
[23] Bradley D, Cresswell TM, Puttock JS. Flame acceleration due to flame-induced instabilities in large-scale explosions. Combust Flame 2001 Mar 1;124(4):551–9. https://doi.org/10.1016/S0010-2180(00)00208-X.
[24] Bauwens CR, Bergthorson JM, Dorofeev SB. Critical Peclet numbers for the onset of Darrieus-Landau instability in atmospheric-pressure methane-air flames. In: Proc 25th ICDERS; 2015 Aug 2. p. 2–7. Leeds, UK, August, http://www.icders.org/ICDERS2015/abstracts/ICDERS2015-231.pdf.
[25] Gillespie L, Lawes M, Sheppard CG, Woolley R. Aspects of laminar and turbulent burning velocity relevant to SI engines. SAE Trans 2000 Jan 1:13–33. https://www.jstor.org/stable/44634200.
[26] Bradley D, Lawes M, Mumby R, Ahmed P. The stability of laminar explosion flames. Proc Combust Inst 2019 Jan 1;37(2):1807–13. https://doi.org/10.1016/j.proci.2018.07.067.
[27] Gostintsev YA, Istratov AG, Shulenin YV. Self-similar propagation of a free turbulent flame in mixed gas mixtures. Combust Explos Shock Waves 1988 Sep;24(5):563–9. https://doi.org/10.1007/BF00755496.
[28] Bradley D. Instabilities and flame speeds in large-scale premixed gaseous explosions. Philos Trans R Soc London, Ser A: Math Phys Eng Sci 1999 Dec 1;357(1764):3567–81. https://doi.org/10.1098/rsta.1999.0510.
[29] Bradley D, Hicks RA, Lawes M, Sheppard CGW, Woolley R. The measurement of laminar burning velocities and Markstein numbers for iso-octane–air and iso-octane–n-heptane–air mixtures at elevated temperatures and pressures in an explosion bomb. Combust Flame 1998;115(1–2):126–44. https://doi.org/10.1016/S0010-2180(97)00349-0.
[30] Gu XJ, Haq MZ, Lawes M, Woolley R. Laminar burning velocity and Markstein lengths of methane–air mixtures. Combust Flame 2000 Apr 1;121(1–2):41–58. https://doi.org/10.1016/S0010-2180(99)00142-X.
[31] Bradley D, Lawes M, Mumby R. Cellular flame instabilities. InProceedings of the eighth international seminar on fire and explosion hazards (ISFEH8). USTC Press; 2017 Sep 1. p. 579–87. https://doi.org/10.20285/c.sklfs.8thISFEH.058.
[32] Clavin P. Dynamic behavior of premixed flame fronts in laminar and turbulent flows. Prog Energy Combust Sci 1985 Jan 1;11(1):1–59. https://doi.org/10.1016/0360-1285(85)90012-7.
[33] Bechtold JK, Matalon M. Hydrodynamic and diffusion effects on the stability of spherically expanding flames. Combust Flame 1987 Jan 1;67(1):77–90. https://doi.org/10.1016/0010-2180(87)90015-0.
[34] Göttgens J, Mauss F, Peters N. Analytic approximations of burning velocities and flame thicknesses of lean hydrogen, methane, ethylene, ethane, acetylene, and propane flames. InSymposium (International) on Combustion 1992 Jan 1;24(1):129–35. https://doi.org/10.1016/S0082-0784(06)80020-2. Elsevier.
[35] Palacios A, Bradley D. Conversion of natural gas jet flame burners to hydrogen. Int J Hydrogen Energy 2021 May 13;46(33):17051–9. https://doi.org/10.1016/j.ijhydene.2021.02.144.
[36] Bradley D, Gaskell PH, Gu XJ. Burning velocities, Markstein lengths, and flame quenching for spherical methane-air flames: a computational study. Combust Flame 1996 Jan 1;104(1–2):176–98. https://doi.org/10.1016/0010-2180(95)00115-8.
[37] Bradley D, Lawes M, Morsy ME. Flame speed and particle image velocimetry measurements of laminar burning velocities and Markstein numbers of some hydrocarbons. Fuel 2019 May 1;243:423–32. https://doi.org/10.1016/j.fuel.2019.01.067.
[38] Law CK, Jomaas G, Bechtold JK. Cellular instabilities of expanding hydrogen/propane spherical flames at elevated pressures: theory and experiment. Proc Combust Inst 2005 Jan 1;30(1):159–67. https://doi.org/10.1016/j.proci.2004.08.266.
[39] Bradley D, Lawes M, Morsy ME. Measurement of turbulence characteristics in a large scale fan-stirred spherical vessel. J Turbul 2019 Mar 4;20(3):195–213. https://doi.org/10.1080/14685248.2019.1610566.
[40] Morsy ME, Yang J. Numerical and experimental study on turbulence statistics in a large fan-stirred combustion vessel. Exp Fluid 2021 May;62(5):1–20. https://doi.org/10.1007/s00348-021-03212-9.
[41] Morley C. Gaseq: a chemical equilibrium program for Windows. Ver. 0.79. 2005.
[42] Bradley D, Sheppard CG, Suardjaja IM, Woolley R. Fundamentals of high-energy spark ignition with lasers. Combust Flame 2004 Jul 1;138(1–2):55–77. https://doi.org/10.1016/j.combustflame.2004.04.002.
[43] Kwon OC, Rozenchan G, Law CK. Cellular instabilities and self-acceleration of outwardly propagating spherical flames. Proc Combust Inst 2002 Jan 1;29(2):1775–83. https://doi.org/10.1016/S1540-7489(02)80215-2.
[44] Taylor SC. Burning velocity and the influence of flame stretch (Doctoral dissertation, University of Leeds). https://etheses.whiterose.ac.uk/2099/.
[45] Halter F, Chauveau C, Djebaïli-Chaumeix N, Gökalp I. Characterization of the effects of pressure and hydrogen concentration on laminar burning velocities of methane–hydrogen–air mixtures. Proc Combust Inst 2005 Jan 1;30(1):201–8. https://doi.org/10.1016/j.proci.2004.08.195.
[46] Vu TM, Park J, Kwon OB, Kim JS. Effects of hydrocarbon addition on cellular instabilities in expanding syngas–air spherical premixed flames. Int J Hydrogen Energy 2009 Aug 1;34(16):6961–9. https://doi.org/10.1016/j.ijhydene.2009.06.067.